



Article

Characterization of Nano-Mechanical, Surface and Thermal Properties of Hemp Fiber-Reinforced Polycaprolactone (HF/PCL) Biocomposites

Hom Nath Dhakal ^{1,*}, Sikiru Oluwarotimi Ismail ², Johnny Beaugrand ^{3,4}, Zhongyi Zhang ¹ and Jurgita Zekonyte ¹

¹ Advanced Materials and Manufacturing (AMM) Research Group, School of Mechanical and Design Engineering, University of Portsmouth, Portsmouth PO1 3DJ, UK; zhongyi.zhang@port.ac.uk (Z.Z.); jurgita.zekonyte@port.ac.uk (J.Z.)

² Department of Engineering, Centre for Engineering Research, School of Engineering and Computer Science, University of Hertfordshire, Hatfield AL10 9AB, UK; s.ismail3@herts.ac.uk

³ INRAE, UMR614 Fractionnement des AgroRessources et Environnement, F-51686 Reims, France; johnny.beaugrand@inrae.fr

⁴ INRAE, Research Unit BIA UR1268, Rue Geraudiere, F-44316 Nantes, France

* Correspondence: hom.dhakal@port.ac.uk; Tel.: +44-(0)23-9284-2582

Received: 18 March 2020; Accepted: 6 April 2020; Published: 10 April 2020



Abstract: The quest for sustainable, low-cost and environmental friendly engineering materials has increased the application of natural fiber-reinforced polymer (FRP) composite. This paper experimentally investigates the effects of variable mean hemp fiber (HF) aspect ratios (ARs) of 00 (neat), aspect ratios AR_19, AR_26, AR_30 and AR_38 on nano-mechanical (hardness, modulus, elasticity and plasticity), surface and thermal properties of hemp fiber/polycaprolactone (HF/PCL) biocomposites. These biocomposites were characterized by nanoindentation, contact angle, surface energy, thermogravimetric analysis (TGA), thermal conductivity and differential scanning calorimetry (DSC) techniques. After nanoindentation and thermal conductivity tests, the results obtained evidently show that the HF/PCL sample with aspect ratio (AR_26) recorded optimal values. These values include maximum hardness of approximately 0.107 GPa, elastic modulus of 1.094 GPa, and plastic and elastic works of 1.580 and 1.210 nJ, respectively as well as maximum thermal conductivity of 0.2957 W/mK, when compared with other samples. Similarly, the optimal sample exhibits highest main degradable temperature and degree of crystallinity of 432 °C and 60.6%, respectively. Further results obtained for the total surface energies and contact angles of these samples with glycerol and distilled water are significant for their materials selection, design, manufacturing and various applications.

Keywords: polycaprolactone; hemp fibre; biocomposites; contact angle measurements; nanoindentation; nano-mechanical properties; surface energy; thermal stability

1. Introduction

Hemp fibers are abundantly available, sustainable, renewable and biodegradable. Hemp fibers have some outstanding mechanical properties (mainly tensile strength at break and tensile modulus) when compared with other naturally available plant fibers, such as date palm, jute, flax, to mention but a few [1–4]. These fibers have a good environmental impact, especially when compared with conventional fibers, such as glass [5]. These attractive attributes have resulted into an increased use of these fibers as reinforcements in composite materials. These bast fibers such as hemp and flax provide good acoustic insulating properties due to their hollow structure. During their processing stages, lesser energy is required when compared to the synthetic (carbon and glass) fiber-reinforced

polymer (FRP) composites. However, natural (hemp) fibers attract few drawbacks. These include the lack of confidence in the use and performance of natural plant fiber and their composites and low degradation temperature, which is about 230 °C [6]. Poly(ϵ -caprolactone) (PCL) is a biodegradable matrix, semi-crystalline, non-cytotoxic polyester.

Reported works on natural fibers as reinforcement in composites have revealed that the shortcomings such as less compatible with hydrophobic matrices, natural variability, low processing temperatures and comparatively lower mechanical properties in comparison to conventional glass and carbon fibre reinforcements have been minimised by modifying fiber surfaces using various treatments. These different modification methods have helped achieving improvements in physical, mechanical and thermal properties of various natural fibres by making fibers compatible with different polymer matrices [7,8]. In addition to these techniques, fiber aspect ratio (AR), which is determined as length divided by diameter of the fiber (l/d), is one of the significant factors that determines the mechanical properties of the polymer matrix composites (PMCs) [9]. Therefore, effects of variable hemp fiber ARs on some important properties are investigated in this present paper.

Few experimental studies have been reported on mechanical properties of biocomposites. Dhakal et al. [10] investigated into the effects of low-velocity impact from falling on jute/methacrylated soybean oil bio-composites. Four different types of samples, different fiber geometry and various thicknesses were impacted and they reported that the biocomposites displayed satisfactory impact resistance behavior. Furthermore, another reported works on composites based on biodegradable PCL matrices and reinforced with lignocellulosic reinforcements have suggested that the biocomposites displayed comparable mechanical properties to that of conventional-based matrices. The influence of the extrusion parameters on the fiber length evolution along the screw profile on hemp fiber-reinforced poly (ϵ -caprolactone)-based biocomposites was investigated [11]. They suggested that fiber length was rapidly decreased after introduction of the fiber and during the flow through the kneading blocks. A recent comprehensive work on amorphized cellulose as filler in biocomposites based on PCL has been reported [12].

The properties of fiber-reinforced composites depend on many factors. These factors include, but are not limited to, types of matrices and reinforcement used, fiber volume fraction, fiber AR, fiber dimensions and interfacial adhesion between reinforcement and the matrix. At low AR, the addition of reinforcement into the composite can create the phase of discontinuity leading to structural heterogeneity and can result in poor mechanical performance. At higher AR up to its threshold, the mechanical properties are expected to increase as a result of good interfacial interaction between the matrix and the reinforcement [13]. In addition, both thermo-mechanical and morphological properties (flexural, damping at temperature interest of 80 °C) of chopped industrial hemp fiber-reinforced cellulosic plastic biocomposites have been improved, especially with 30% plasticized polar cellulose acetate plastic (CAP) [14].

Furthermore, the mechanical properties (tensile and flexural) of woven natural (banana) fiber with Musaceae/epoxy composite materials have been experimentally analyzed [15]. They obtained maximum values of stress and Young's modulus in both x and y -directions. An evaluation of the mechanical properties of natural coir fiber-reinforced epoxy composite has been similarly reported [16]. Their results indicated coir as a promising reinforcing fiber for producing low load bearing thermoplastic FRP composite.

The nanoindentation technique is commonly used to analysis the surface properties of materials, such as coated surface [17]. It has been extensively used to evaluate the mechanical behavior of different polymers [18–20] and nano-composites [21–28]. Perrier et al. [29] reported the influence of water ageing on nanoindentation response of the in situ components of hemp yarn/epoxy composites. Nanomechanical properties (hardness and elastic modulus) of layered silicate-reinforced unsaturated polyester nanocomposites was studied [23], using nanoindentation technique. They reported that the nanoindentation properties of the nanocomposites were enhanced, caused by clay reinforcement and the amount of clay dispersion within the unsaturated polymer resin. The nanomechanical

properties (creep, hardness and elastic modulus) behavior of human hair using the nanoindentation and scanning electron microscopy (SEM) techniques was studied [30]. They reported that hair follicle recorded the greater hardness and elastic modulus than cortex at lateral direction, while the depth of indentation increased as both the elastic modulus and hardness of the hair decreased. Similar to this study, the mechanical properties of short flax fiber-reinforced polypropylene compounds were investigated [31]. Both strength and stiffness of the compound were achieved with the reinforcing flax fiber as well as effective compactible fiber-matrix interaction.

Furthermore, mechanical, water absorption and thermal conductivity properties of hemp fiber reinforced polyurethane composites have been investigated [32]. The experimental result suggested a promising application of these sustainable composites in thermal insulation field, due to their improved mechanical properties. The thermo-physical properties of natural fiber (banana/sisal), hybrid pineapple leaf and glass fibers-reinforced polyester composites have been investigated [33]. The composite thermal contact resistance was reduced due to the chemical treatment of the fibers, while a significant improved heat transfer ability was achieved with the hybridised natural fiber with glass. The effects of phenylphosphate-based flame retardant on flammability, thermal stability and mechanical properties of glass fiber-reinforced epoxy (GRE) composites have been investigated [34]. The hardness and Young's modulus of the epoxy (EP) matrix was performed using a nanoindentation test. They reported that N'-diamyl-p-phenylphosphonicdiamide (P-MA) had no effect on the hardness of the EP matrix and the interfacial strength of glass fiber/epoxy matrix.

In addition, some studies have been conducted on contact angle and surface energy analysis of different materials [6,35–37]. For instance, the effect of fiber treatment and glass fiber hybridisation on thermal degradation and surface energy behavior of hemp fiber/unsaturated polyester (HF/UP) composites has been studied [6], using thermogravimetric analysis (TGA) and contact angle measurement. Their experimental results indicated the possibility of obtaining better thermal stability and wetting behavior of HF/UP composites with surface treatment and hybridisation techniques. Similarly, analysis of both contact angle and surface energy of soy materials subjected to potassium permanganate (KMnO_4) oxidation and autoclave treatment has been conducted [35].

Based on the extant, extensive and aforementioned literature, there is no comprehensive report on thermal (stability and conductivity), surface (energy and contact angle) and nano-mechanical properties (hardness, modulus, elasticity and plasticity) of a complete biodegradable and biocomposite using thermogravimetric analysis, differential scanning calorimetry and nanoindentation techniques, concomitantly. Importantly, the effects of variable hemp fiber aspect ratios (ARs) of 00 (neat), 19, 26, 30 and 38 on these notable properties of the HF/PCL composite samples are extensively investigated. Therefore, this paper characterises the nano-mechanical, surface and thermal properties of natural and biodegradable hemp fiber-reinforced PCL biocomposites.

Composite parts fabricated by using non-renewable reinforcements such as glass fibre are heavy as well as poor acoustic and damping properties. The bio-composites based on PCL reinforced using fibres such as hemp not only provide weight saving (lightweighting), but also provide improved environmental sustainability than glass fibres. The hemp/PCL based biocomposites investigated in this study can be applied in producing non-structural interior parts.

2. Experimental Procedures

2.1. Materials

A semi crystalline polymer and non-cytotoxic polyester, known as polycaprolactone, with molecular weight of 80 kgmol^{-1} was used as a matrix. It is a biodegradable polymer with low melting temperature of approximately 60°C . A lignocellulosic hemp fiber was used as reinforcement. It was harvested in Aube, France and supplied by FRD©, and melt with PCL Perstop (UK) (Capa© 6800), to produce a completely biodegradable, sustainable, renewable, recyclable and environmentally friendly HF/PCL biocomposite samples.

2.2. Fabrication of Neat Poly(ϵ -Caprolactone) (PCL) and Hemp Fiber (HF)/PCL Biocomposite Samples

The small bundles of scutched bast hemp fibers were manually cut to a length of nearly 20 mm, prior to its processing stage. Laminates were obtained by press moulding from both extrudate neat PCL (AR_00) or 20% wt. hemp fiber/PCL composites differing in their average L/d ratio. The press used was a two-column automatic laboratory hydraulic press (Carver, Wabash, IN USA) equipped with heating platens. The mould (MGTS, La Neuville, France) dimension was 20 cm \times 20 cm length and 5 cm thickness, filled with samples and preheated for 5 min at 135 °C before 1 Ton pressing for 3 min. This is required to ensure homogeneity of the fibers. Therefore, after twin screw extrusion and fabrication of the laminates, the mean fiber element diameter, d (μm) was approximately 22 μm , while the mean fiber element lengths, l (μm) were 432, 568, 708 and 845 μm to produce fiber ARs of 19, 26, 30 and 38, respectively, including AR_00 (neat PCL matrix, without hemp fiber/reinforcement). The average length of the fibers elements for the non-extruded fiber batch was measured by image analyses from 2D high-resolution scanner. A Clextral BC 21 laboratory scale twin extrusion machine was used for the fabrication. This machine has a length and diameter of 900 and 20 mm, respectively. As shown in Figure 1, both hemp fibers and the PCL matrix were introduced into the machine through the two-hopper location, the hemp fibers were added to the melted PCL matrix in order to prevent severe extrusion conditions, during the fabrication of the HF/PCL biocomposite laminate samples. These samples were further cut into samples for nanoindentation, thermogravimetric analysis and differential scanning calorimetry tests.

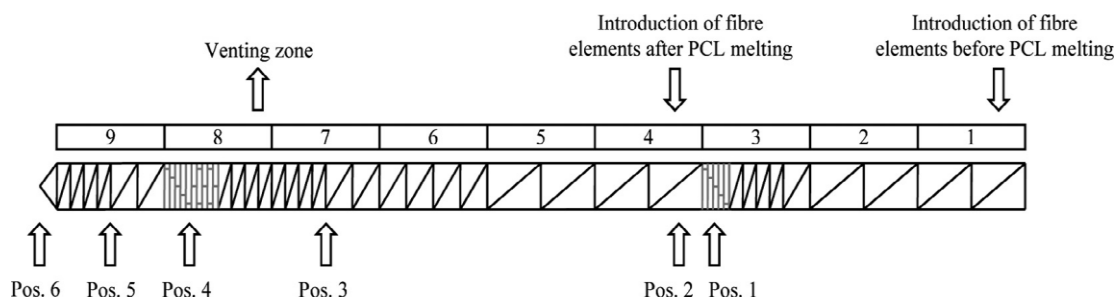


Figure 1. Clextral BC 21 Screw profile used in sample fabrication process, showing positions of introducing hemp fibers before and after poly(ϵ -caprolactone) PCL melting as well as venting zone on the twin screw extrusion machine.

2.3. Nanoindentation Test

The nanoindentation tests were performed using commercially available Nano TestTM (Micro Materials, Wrexham, U.K.) apparatus, with a Berkovich (three-sided pyramidal diamond) indenter. The schematic diagrams and illustrations of the nanotest system, a typical Berkovich indenter tip and 16 symmetrical indentations (4 \times 4 matrix, 30 μm apart) are shown in Figure 2a–c, respectively. Each of the four nanoindentation test samples has dimension of 20 mm \times 20 mm \times 6 mm. With suitable adhesive, the samples were mounted to the nanoindentation fixture and all the tests were performed at room temperature. The tests were conducted in load controlled mode using the following experimental indentation parameters: initial load of 0.1 mN, maximum load of 15 mN for all indents, dwell time (holding time) of 5 s at maximum load, loading and unloading rate of 2.00 mN/s.

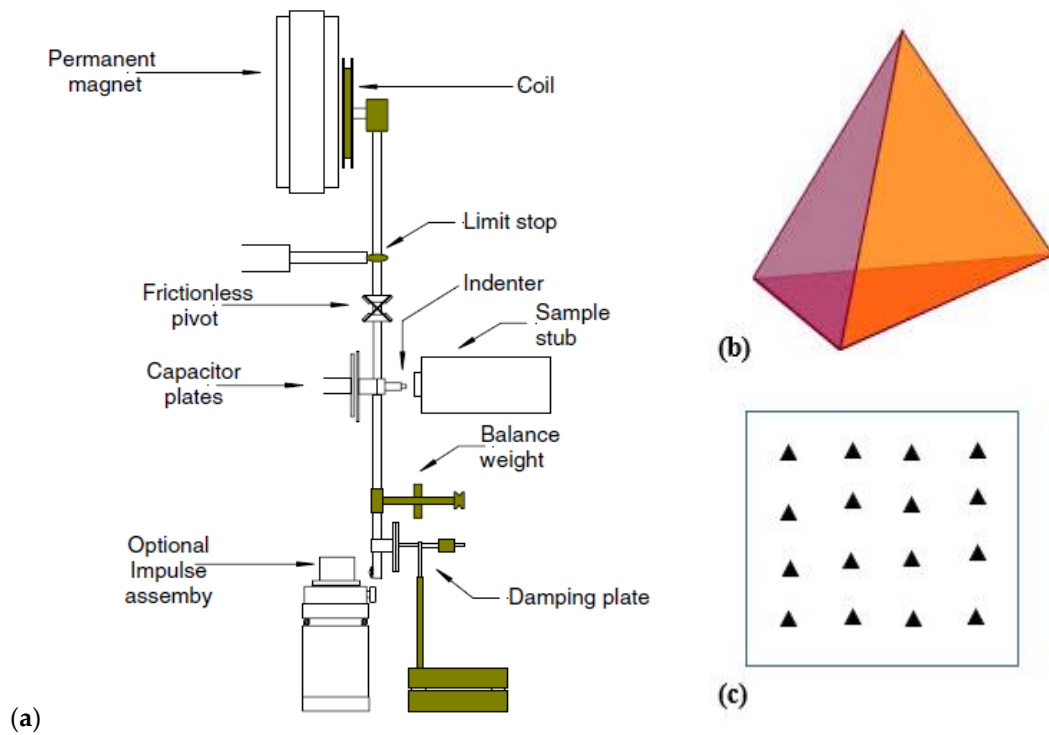


Figure 2. (a) Diagrammatic illustration of the nanoindentation test system, (b) a typical Berkovich indenter tip for nanoscale measurements and (c) symmetrical indentations at 30 μm apart (not to scale) on the HF/PCL biocomposite sample.

2.4. Analysis of Nanoindentation Quantities

Figure 3, adapted from Shokrieh et al. [27], illustrates the schematic representation of a complete evolution of typical loading-unloading cycle. This indentation cycle depicts the maximum test load or force (P_{max}), maximum depth (h_{max}), final depth after loading (h_f) and the slope (S) of the unloading curve (Equations (1) and (2)). This slope is referred to as the elastic contact or unloading stiffness of the sample. Loading-unloading curves were analysed using the Oliver-Phar method [38] with the software provided by Micromaterials. The hardness, H and the reduced elastic modulus, E_r are defined by Equations (1) and (2), respectively:

$$H = \frac{P_{max}(h_{max})}{A(h_c)} \quad (1)$$

where A and h_c are the contact area (between the indenter and the sample) at maximum load and contact depth, respectively;

$$E_r = \frac{S}{2\beta} \sqrt{\frac{\pi}{A(h_c)}} \quad (2)$$

where β is a correction factor which varies slightly for various indenter geometry (1.034 for a Berkovich indenter) and $S = \frac{dP}{dh}$. The reduced elastic modulus accounts for the elastic displacement of both indenter and sample. The elastic modulus of the sample, E_s can be derived from the reduced elastic modulus, E_r (from the tests) and the indenter elastic modulus, E_i (usually 1141 GPa for the diamond) by Equation (3):

$$\frac{1}{E_r} = \frac{(1 - v_s^2)}{E_s} + \frac{(1 - v_i^2)}{E_i} \quad (3)$$

where v_s and v_i are Poisson's ratios of the polymer sample and diamond indenter tip respectively, approximately 0.2 for polymer and 0.07 for diamond. The diamond indenter tip is much stiffer than

polymer sample ($E_s \ll E_i$). Therefore, Equation (3) can be reduced to $\frac{1}{E_r} \approx \frac{(1-\nu_s^2)}{E_s}$ and $h_c = h_{max} - \varepsilon \cdot \frac{P_{max}}{S}$, where ε depends on the shape of the indenter tip (usually 0.75 is recommended for a Berkovich indenter) and $h_{max} \leq 200$ nm for nano range [39,40]. However, from Equation (3), elastic modulus of the sample, E_s can be expressed as:

$$E_s = \frac{1 - \nu_s^2}{\frac{1}{E_r} - \frac{1 - \nu_i^2}{E_i}} \quad (4)$$

The mean values of the concerned experimental nanoindentation data obtained from the loading–unloading curves of the tests performed at a peak indentation load of 15 mN are later presented and discussed extensively.

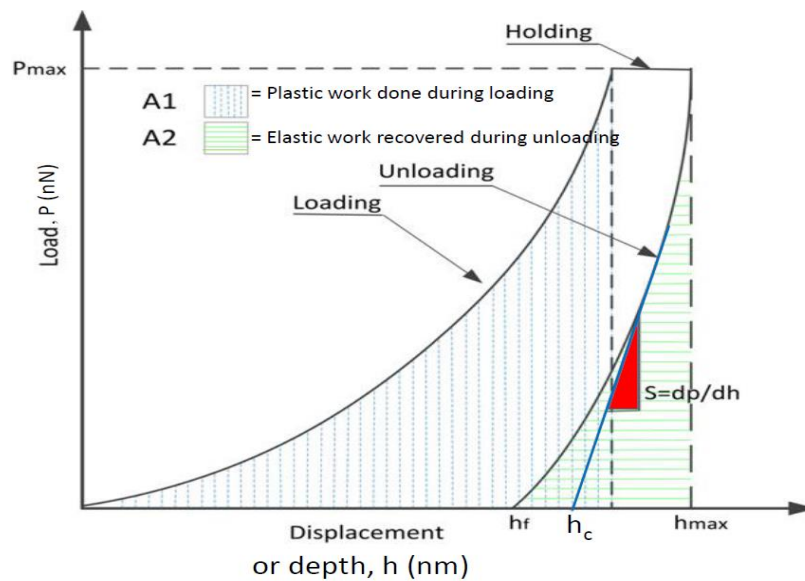


Figure 3. The evolution of the nanoindentation test, showing a typical load–displacement curve and loading–unloading cycle.

2.5. Thermal Stability Analysis

As a result of the wide range of applications of composite materials, including thermal insulators, engine covers and body of automobiles and air/space crafts, to mention but a few, there is need for further investigation of the thermal stability of the 5 samples for better characterization of their properties and effective applications.

2.5.1. Thermogravimetric Analysis (TGA)

TGA was performed using a TGA2950 (TA Instrument, Paris, France). The samples were placed in a platinum crucible, and heated in a nitrogen filled environment at the heating rate of 10 °C/min from ambient temperature to 600 °C. The initial weights of the samples were approximately 12 mg. The data from the test is displayed as TG (weight loss as a function of temperature) and DTG (derivative thermal gravimetry, weight loss rate as a function of temperature).

2.5.2. Differential Scanning Calorimetry (DSC)

Differential scanning calorimetry (DSC) experiments were performed on hemp fiber/PCL biocomposite samples with a DSC Q100 (TA Instrument, Paris, France) in aluminium pans. The following parameters were used:

1. Equilibrate at −15 °C
2. Isothermal for 1 min

3. Ramp 5.00 °C/min to 120 °C
4. Cooling: Non regulated section (decrease between 10 and 15 °C/min) [41]
5. Isothermal for 1 min
6. Ramp 10 °C/min to 120 °C.

2.5.3. Thermal Conductivity

The quick thermal conductivity meter QTM-500 (Kyoto Electronic Manufacturing Company, Tokyo, Japan) consisted of a thermocouple, and a single heater wire was used. Its operating principle was based on the temperature variation (increase or rise) when applying constant electric power to the heater and thus the wire. This rise in temperature has an exponential shape. The temperature values occurred during the experiment were recorded and plotted in a linear form (taking the logarithm of the exponential one). Various important properties were derived and drawn from the linear plot of the temperature values. Therefore, from the linear plot obtained and the angle, the thermal conductivity is determined using Equation (5):

$$\lambda = \frac{q \cdot \ln \frac{t_{i+1}}{t_i}}{4\pi(T_{i+1} - T_i)} \quad (5)$$

where; λ = specimen thermal conductivity (W/mK), q = generated heat per unit length of specimen/time (W/m), t_i and t_{i+1} = measured time length (s), T_i and T_{i+1} = temperature values at t_i and t_{i+1} , respectively (K). The test was performed according to the standards ASTM C177 [32] and in different directions to derive the average values.

2.6. Contact Angle and Surface Energy Determination

A computer-controlled KSV 101 optical contact angle meter (CAM) (KRÜSS GmbH, Hamburg, Germany) was used to determine the contact angle and surface energy of the 5 hemp/PCL biocomposite samples. It captured and analysed video images automatically in order to measure the dynamic or static contact angles, the surface tension of liquids, surface free energies and absorption of liquids. Both water and glycerol were used as the test fluids or liquid probes, with known polar and dispersive components of surface tension. The thermodynamics of solid–liquid interactions are analysed from the measurements of contact angle data obtained. From Young's equation [42], solid surface tension from contact angle is obtained in Equation (6):

$$\gamma_s = \gamma_l \cos \theta + \gamma_{sl} \quad (6)$$

where θ represents the probe liquid contact angle, γ_s and γ_l denote the solid and liquid surface tensions or free energy respectively and γ_{sl} indicates the solid–liquid interfacial free energy. θ and γ_l are the only measurable quantities in Young's equation. An additional relationship known as geometric mean is required to obtain both γ_s and γ_{sl} . This relationship is obtained by combining Young's equations using Fowke's proposed model or approach [35,43,44]:

$$\gamma_l(1 + \cos \theta) = 2 \left[\sqrt{(\gamma_l^p * \gamma_s^p)} + \sqrt{(\gamma_l^d * \gamma_s^d)} \right] \quad (7)$$

where γ_l^p and γ_s^p represent the liquid and solid polar surface energy, respectively and γ_l^d and γ_s^d liquid and solid dispersive surface energies, respectively. The total surface energy is the addition of the polar and dispersive surface tensions or energies. Therefore, Equation (7) was used to determine both two components (dispersive and polar) of the total surface free energy of all the 5 biocomposite samples. This was based on the measurements from the contact angle of 20 drops averaged for each of the liquids, using KSV contact angle meter (CAM) surface free energy (SFE) software. Similarly, the solid surface was characterised by determining free surface energy.

2.7. Scanning Electron Microscopy (SEM)

The morphological analysis of the biocomposites was performed by using scanning electron microscopy (SEM) JSM/JEOL 6100 (Jeol Ltd., Tokyo, Japan) at room temperature. The samples were then placed on stands and coated with gold palladium to enhance the conductivity during imagery.

3. Results and Discussion

3.1. Nanoindentation Behavior

The average values of the nanoindentation experimental results obtained are summarized and tabulated in Table 1. The samples exhibit a similar, continuous and consistent loading, holding period and unloading stages, but at different loads and depth. With an increase in the fiber ARs of the samples, the material resistance to nanoindentation is found to be different. The maximum hardness and reduced elastic modulus of nearly 0.107 GPa and 1.094 GPa were recorded by sample AR_26 and sample AR_38 has the minimum hardness and reduced elastic modulus values of 0.073 GPa and 0.540 GPa respectively. This implies that sample AR_26 has the highest resistance to material plastic deformation.

Table 1. Nano-mechanical properties of the samples after nano-indentation test, with standard deviation.

Samples	Hardness (GPa)	Reduced Modulus (GPa)	Elastic Recovery (mm)	Plastic Work (nJ)	Elastic Work (nJ)	Maximum Depth (nm)	Plastic Depth (nm)
AR_00	0.0820	0.5457	0.3886	0.98	1.05	1855.46	1336.42
(Neat)	(±0.009)	(±0.042)	(±0.019)	(±0.086)	(±0.115)	(±8.12)	(±20.32)
AR_19	0.0882	1.0893	0.2083	1.40	0.94	1820.97	1507.39
	(±0.006)	(±0.135)	(±0.017)	(±0.145)	(±0.050)	(±8.40)	(±24.58)
AR_26	0.1066	1.0936	0.2510	1.58	1.21	1815.58	1451.56
	(±0.009)	(±0.127)	(±0.018)	(±0.220)	(±0.107)	(±6.43)	(±23.08)
AR_30	0.0903	0.9433	0.2448	1.43	1.08	1852.19	1488.63
	(±0.013)	(±0.116)	(±0.026)	(±0.226)	(±0.182)	(±35.87)	(±44.00)
AR_38	0.0726	0.5403	0.3470	0.95	0.93	1841.73	1367.43
	(±0.004)	(±0.026)	(±0.015)	(±0.080)	(±0.072)	(±12.70)	(±17.72)

From the trend of the results presented in Table 1, it is observed that the both nano-mechanical (nanoindentation) hardness and reduced elastic modulus properties of the 5 samples were increased till maximum and threshold sample AR_26 were obtained. After this optimal sample, these two important properties began to decline until the least values were recorded by the sample AR_38, with highest fiber AR. Also, both hardness and elastic modulus of the samples determined the contact depth, as these properties decreased with an increasing contact depth among the HF/PCL biocomposite samples, especially with higher AR samples. Comparatively, it was evident that hemp fiber has a clear reinforcement effect on the PCL matrix, as observed by the increased hardness (+30%) and modulus (+100.39) of sample AR_26 when compared with the neat PCL sample AR_00. This can be attributed to the best intermolecular interaction and interfacial properties between PCL and hemp fiber AR_26, as depicted in Figure 4a,b.

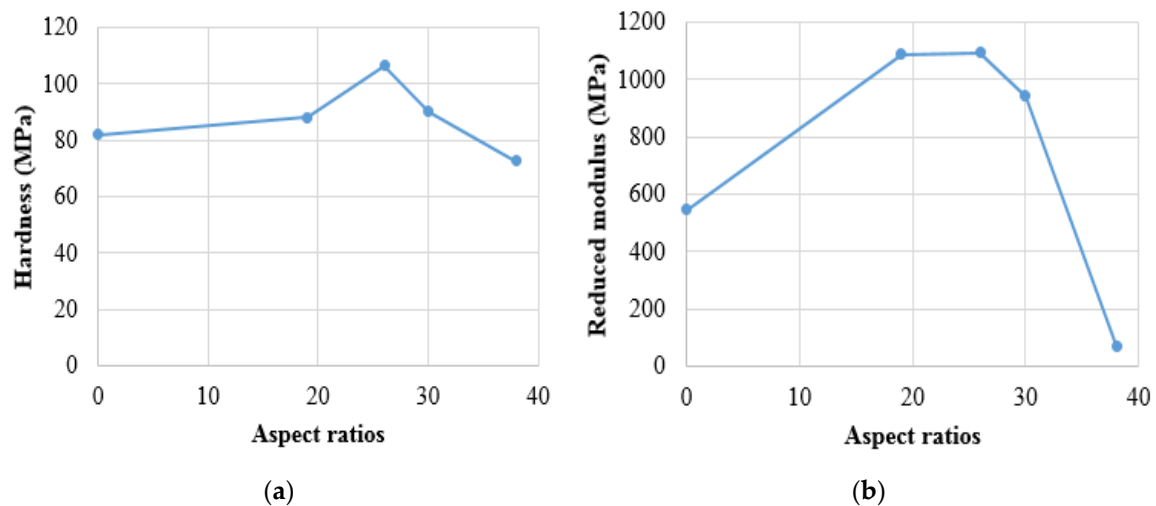


Figure 4. Effects of aspect ratios on (a) hardness (b) reduced modulus.

In addition, other properties such as elastic and plastic works of the samples recorded similar trend, having maximum values of nearly 1.21 nJ and 1.58 nJ respectively with sample AR_26. With these optimal properties, sample AR_26 was expected to possess the least indentation depth, which was approximately 1816 nm. The neat PCL recorded the highest indentation depth of nearly 1856 nm. The average maximum depth recorded by all the samples at peak load was approximately 1840 nm. These results are in close agreement with that of Aldousiri et al. [25]. They used spent neat polyamide and layered silicate as matrix and filler/reinforcement materials, respectively. Moreover, the plastic work was done during the loading stage of the indenter inside the samples, while the elastic work was recovered during the unloading stage, as previously and graphically illustrated in Figure 3. Furthermore, a small change, commonly known as ‘pop out’ and ‘elbow’ in the unloading load-depth curves only occurred from all the samples, towards the end of the cycle. This phenomenon has been similarly observed by Singh et al. [45,46] and associated with the Berkovich indenter [47] and phase transformation of materials [48].

3.2. Thermal Properties: Thermogravimetric, Differential Scanning Calorimetry and Conductivity Analysis

3.2.1. Thermal Stability

The results obtained for both TGA and DSC were discussed to further characterize the damage responses of the samples. The temperature of the main degradation peaks obtained from TGA test for all samples are illustrated in Table 2. The data recorded for hemp fiber/PCL show a clear decrease of the degradation peak temperature (close to 10 °C) compared to the PCL matrix, especially marked for the highest ARs of 30 and 38. It is clearly evident that the closest value of degradation temperature, to the neat PCL sample with highest value, was obtained with the HF/PCL biocomposite sample of AR of 26. The results of thermal stability of the neat PCL matrix are very similar to the result obtained by Cocca et al. [49] and significantly affected with the hemp fiber reinforcement, as shown in Figure 5.

Table 2. Thermogravimetric analysis (TGA) measurements.

Samples	Main Degradation Temperature (°C)
AR_00	433
AR_19	428
AR_26	432
AR_30	424
AR_38	424

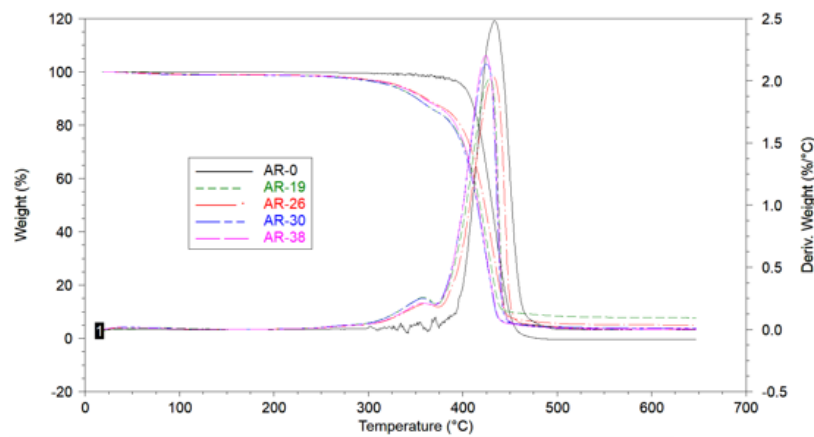


Figure 5. Typical TGA degradation curves of both neat PCL matrix samples (AR_00) and HF/PCL biocomposite samples (AR_19, 26, 30 and 38), showing the effect of fiber on the degradation properties of the HF/PCL samples.

3.2.2. Crystallization Behavior

TGA results presented in Figure 5 do not clearly show a shift of the temperature of the melting peak (around 58 °C). Hence, there is need for the DSC melting results to further analyse the heat flow (Figure 6). The addition of fibers into the matrix increased the degree of crystallinity of the neat PCL matrix to at least 5%, as illustrated in Table 3. The DSC thermogram of the neat PCL matrix is very similar to the result obtained by Cocca et al. [49]. The degree of crystallinity slightly increased with fibers, which is attributed to acting as nucleating agents for the PCL matrix. It is also evident that the highest increase in crystallinity was observed in the HF/PCL composite sample with AR_26, similar to TGA results. Both TGA and DSC (thermal) results obtained for HF/PCL composite sample with AR_26 could be attributed to its previous optimum and best nano-mechanical properties, as discussed earlier.

Table 3. Differential scanning calorimetry (DSC) melting 1^{er} run.

Samples	Degree of Crystallinity χ (%)
AR_00	50.9
AR_19	55.7
AR_26	60.6
AR_30	56.5
AR_38	58.0

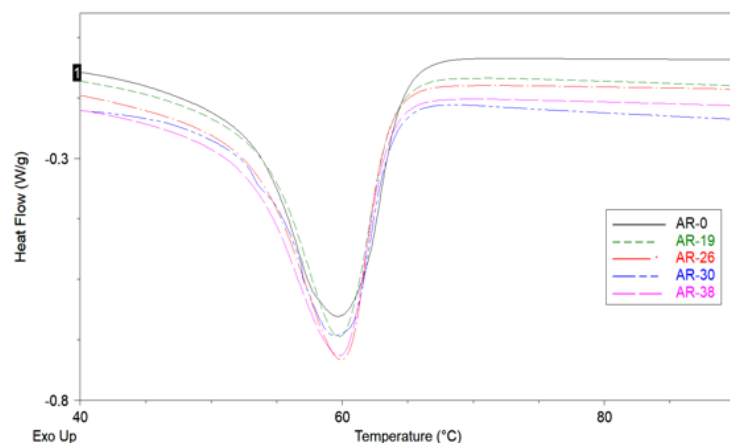


Figure 6. Typical DSC thermograms of both neat PCL matrix samples (AR_0) and hemp/PCL composite samples (AR_19, 26, 30 and 38), depicting the heat flow at an increasing temperature.

3.2.3. Thermal Conductivity

The thermal conductivity is a prominent property that determine the application of thermal insulating materials, as function of parameters such as morphology, homogeneity and density, among others. Figure 7 depicts the average thermal conductivity results of the 5 HF/PCL biocomposites. From the results, the average thermal conductivities for ARs_00 (neat), 19, 26, 30 and 38 samples are 0.2539, 0.2824, 0.2957, 0.2922 and 0.2539 W/mK, respectively. There is no difference in the thermal conductivities of neat PCL (AR_00) and highest AR_38, as both samples recorded the same value of 0.2539 W/mK. This behavior can be attributed to the longest porous structures exhibited by the sample of highest fiber AR_38, with maximum mean fiber element length of nearly 845 μm . There are the presence of central hollows in the multicellular morphology of the bast fibers such as hemp, as depicted in Figure 8. Notwithstanding, it is evident that the thermal conductivity depends on the sample AR. There was an initial increase in the thermal conductivity when hemp fiber was introduced into the PCL matrix, as similarly observed when same hemp fiber and other cellulosic fibers (date palm particles) were added into polyurethane matrix [32,50]. Importantly, it is observed that the thermal conductivities of the samples increased with the hemp fiber AR to a threshold value of 26, after it began to decrease with an increase AR. Therefore, the HF/PCL sample of AR_26 recorded the maximum thermal conductivity of 0.2957 W/mK. This exhibited characteristic could be attributed to the fiber architecture, content, volume fraction as well as properties of the fiber, matrix and their ratios in the optimal sample. These properties include, but are not limited to density of the PCL matrix resin and strength of the embedded fiber present in sample of AR_26. The strength of this optimal sample in terms of thermal stability and nano-mechanical properties has been extensively and previously discussed.

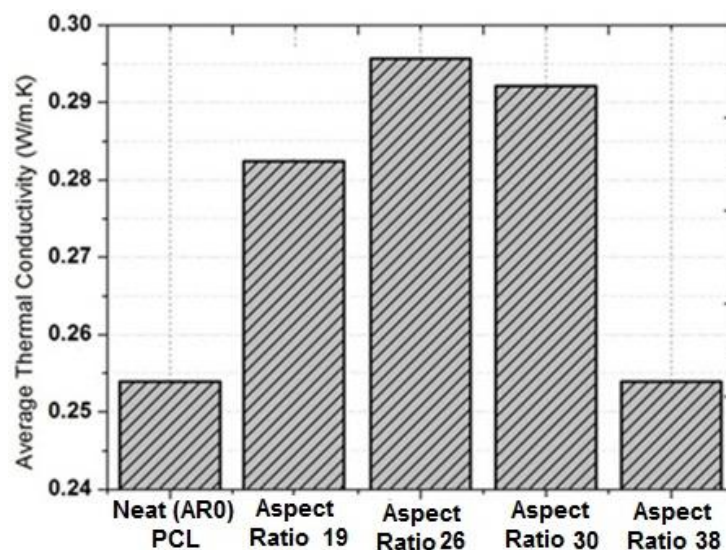


Figure 7. Comparative average thermal conductivities of the 5 samples.

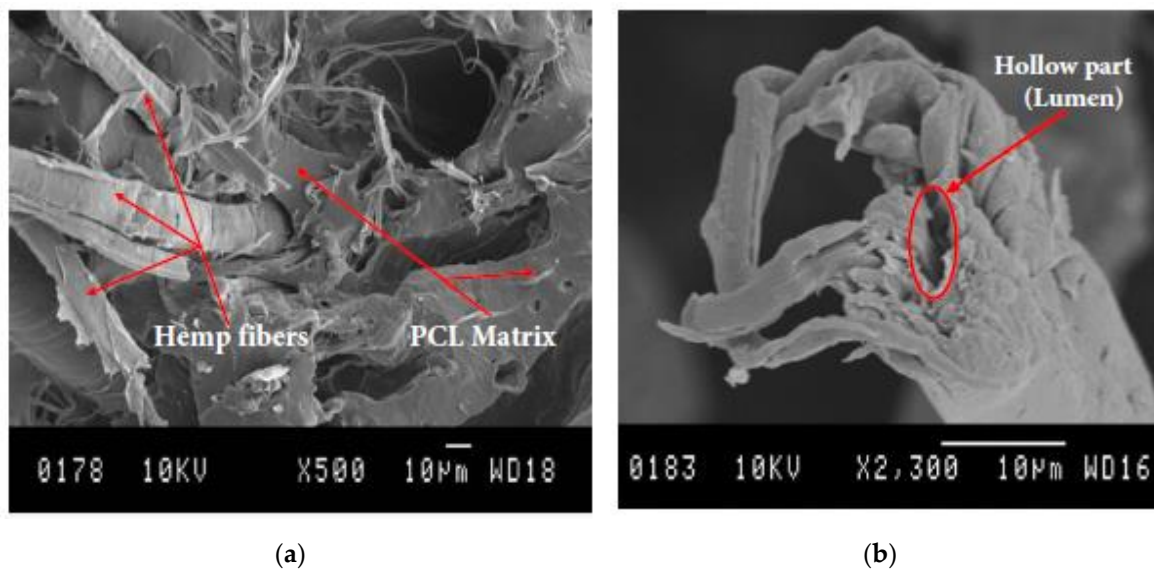


Figure 8. The scanning electron microscope (SEM) micrographs of the (a) hemp fiber and PCL matrix and (b) morphological structure of the bast fiber element (hemp), showing hollow (lumen).

Moreover, the FRP composites are predominantly affected by fiber content, which increased with hemp fiber AR. This implies that hemp fiber possessed higher thermal conductivity than the neat PCL matrix.

Moreover, this sample (AR_26) has the best ability to transfer heat energy through conduction. This property is required during machining operation as much tool-workpiece interfacial temperature is absorbed in order to prevent high tool wear. However, this could lead to high machining-induced damage on the workpiece such as delamination, matrix melting and fiber degradation, if not properly controlled. In addition, material of higher thermal conductivity, such as the HF/PCL biocomposite sample of AR_26 has significant applications potential for electronic packaging and thermal control.

3.3. Contact Angle and Surface Energy Characterization

The wettability of lignocellulosic hemp fiber in liquid matrices plays a significant role in the fabrication of FRP composites, their overall properties and engineering applications. The fiber–matrix adhesion, interfacial bond and strength depend of the wetting behavior. Wettability, hydrophilicity and hydrophobicity are often analysed by the measure of contact angle formed between the materials (HF/PCL biocomposites) and liquids (glycerol and distilled water) used as well as surface energy levels with these liquids. Therefore, the maximum average contact angles for both glycerol and distilled water taken at 1.05 s for all the 5 samples are presented in Table 4 and the total surface energy results for the 2 liquids are illustrated in Table 5.

Table 4. Summary of the contact angle and surface energy results for the 5 samples.

Specimens	Contact Angle (°)	
	Glycerol	Distilled Water
AR_00 *	86.70	94.12
AR_19	93.07	101.95
AR_26	85.21	95.77
AR_30	79.19	86.87
AR_38	87.85	86.65

* AR_00 denotes neat sample, without hemp fiber.

Table 5. Surface tension values of the liquids used.

Liquid	Total Surface Energy (mN/m)
Distilled water	72
Glycerol	64

It is observed that almost all the contact angles from glycerol are less than that of distilled water, and significantly less than 90° . This indicates that glycerol exhibited higher relative wettability, hydrophilicity and adhesion properties with the samples. Consequently, lower total surface energy of 64 mN/m on the surfaces of the samples with glycerol was obtained when compared with 72 mN/m using distilled water. The discrepancy in these values has been similarly reported with water and diiodomethane recorded total surface energies of 72.8 and 50.8 mN/m, respectively [35]. Also, the samples experimentally demonstrated their higher hydrophobic nature with water. It shows that glycerol spread over larger area with smaller contact angles. This phenomenon further shows lower hydrophobicity of most of these samples using glycerol, when compared to distilled water.

4. Conclusions

This experimental paper has comprehensively characterized various nano-mechanical and thermal stability characteristics of biodegradable and sustainable hemp fiber-reinforced PCL biocomposites using nanoindentation, TGA and DSC techniques. Evidently, the effects of variable mean hemp fiber aspect ratios on these properties have been investigated.

From the nanoindentation results obtained, a significant improvement in both hardness and reduced elastic modulus for the biocomposite samples was achieved, with sample AR_26 having the optimal values of hardness and elastic modulus, among other outstanding nanoindentation properties considered. This improvement can be attributed to the hemp fiber AR and the interfacial interaction.

With regard to surface properties, the surface tension values for all samples using glycerol were less than the values obtained from water. This indicated that exposing the samples to glycerol exhibited more wettability than water. In addition, exposure of the samples to water demonstrated a higher hydrophobicity. Furthermore, it was evident that the thermal conductivity of the samples depended on their ARs, as the optimal HF/PCL biocomposite sample of AR_26 recorded the highest average threshold value of 0.2957 W/mK, while both neat (AR_00) and AR_38 samples possessed the lowest average value of 0.2539 W/mK.

Hence, the addition of lignocellulosic hemp fiber into the biodegradable PCL matrix enhanced the properties of the HF/PCL biocomposite samples, when compared with the neat PCL sample. Conclusively, all the results obtained indicated hemp fiber as a promising reinforcing material for making biodegradable, renewable, low-cost and load-bearing thermoplastic biocomposites, significantly with optimal nano-mechanical and thermal properties of sustainable HF/PCL biocomposite sample AR_26. In summary, better knowledge of the properties obtained for these samples is very germane for materials' selection, design, and manufacturing of lightweight parts for various engineering applications.

Author Contributions: H.N.D. contributed in design, conceptualization, analysis and overall communication and writing, J.B. contributed in design, fabrication of samples and thermal analysis, S.O.I. contributed in the experimental work, analysis of results and writing, Z.Z. contributed in experimental and data analysis, J.Z. contributed in review and editing. All authors have read and agreed to the published version of the manuscript.

Funding: This research did not receive any specific grant from funding agencies in the public, commercial, or not-for-profit sectors.

Acknowledgments: The assistance of the following colleagues is greatly and sincerely appreciated: Jean-Eudes Maigret, Miguel Pernes and Alain Lemaitre, INRAE FARE, Reims, France.

Conflicts of Interest: The authors declare no conflict of interest.

References

- Bledzki, A.; Gassan, J. Composites reinforced with cellulose based fibres. *Prog. Polym. Sci.* **1999**, *24*, 221–274. [\[CrossRef\]](#)
- Dhakal, H.N.; Zhang, Z.Y.; Richardson, M.O.W. Effect of Water Absorption on the Mechanical Properties of Hemp Fiber Reinforced Unsaturated Polyester Composites. *Compos. Sci. Technol.* **2007**, *67*, 1674–1683. [\[CrossRef\]](#)
- Mohanty, A.; Misra, M.; Drzal, L.T. Sustainable Bio-Composites from Renewable Resources: Opportunities and Challenges in the Green Materials World. *J. Polym. Environ.* **2002**, *10*, 19–26. [\[CrossRef\]](#)
- Bourmaud, A.; Dhakal, H.N.; Habrant, A.; Padovani, J.; Siniscalco, D.; Ramage, M.H.; Beaugrand, J.; Shah, D.U. Exploring the potential of waste leaf sheath date palm fibres for composite reinforcement through a structural and mechanical analysis. *Compos. Part A Appl. Sci. Manuf.* **2017**, *103*, 292–303. [\[CrossRef\]](#)
- Shahzad, A. Hemp fiber and its composites—A review. *J. Compos. Mater.* **2011**, *46*, 973–986. [\[CrossRef\]](#)
- Dhakal, H.N.; Zhang, Z.Y.; Bennett, N. Influence of Fiber Treatment and Glass Fiber Hybridisation on Thermal Degradation and Surface Energy Characteristics of Hemp/Unsaturated Polyester Composites. *Compos. Part B Eng.* **2012**, *43*, 2757–2761. [\[CrossRef\]](#)
- Mohanty, A.K.; Misra, M.; Hinrichsen, G. Biofibres, biodegradable polymers and biocomposites: An overview. *Macromol. Mater. Eng.* **2000**, *276*, 1–24. [\[CrossRef\]](#)
- Rout, J.; Tripathy, S.S.; Misra, M.; Mohanty, A.; Nayak, S.K. The influence of fiber surface modification on the mechanical properties of coir-polyester composites. *Polym. Compos.* **2001**, *22*, 468–476. [\[CrossRef\]](#)
- Beaugrand, J.; Berzin, F. Lignocellulosic Fibre Reinforced Composites: Influence of Compounding Conditions on Defibrization and Mechanical Properties. *J. Appl. Polym. Sci.* **2013**, *128*, 1227–1238. [\[CrossRef\]](#)
- Dhakal, H.N.; Skrifvars, M.; Adekunle, K.; Zhang, Z. Falling weight impact response of jute/methacrylated soybean oil bio-composites under low velocity impact loading. *Compos. Sci. Technol.* **2014**, *92*, 134–141. [\[CrossRef\]](#)
- Berzin, F.; Vergnes, B.; Beaugrand, J. Evolution of Lignocellulosic Fiber Lengths along the Screw Profile during Twin Screw Compounding with Polycaprolactone. *Compos. Part A Appl. Sci. Manuf.* **2014**, *59*, 30–36. [\[CrossRef\]](#)
- Avolio, R.; Graziano, V.; Pereira, Y.; Cocca, M.; Gentile, G.; Errico, M.; Ambrogio, V.; Avella, M. Effect of cellulose structure and morphology on the properties of poly(butylene succinate-co-butylene adipate) biocomposites. *Carbohydr. Polym.* **2015**, *133*, 408–420. [\[CrossRef\]](#) [\[PubMed\]](#)
- Hull, D.; Clyne, T. *An Introduction to Composite Materials*; Cambridge University Press, (CUP): Cambridge, NY, USA, 1996.
- Wibowo, A.; Mohanty, A.K.; Misra, M.; Drzal, L.T. Chopped Industrial Hemp Fiber Reinforced Cellulosic Plastic Biocomposites: Thermomechanical and Morphological Properties. *Ind. Eng. Chem. Res.* **2004**, *43*, 4883–4888. [\[CrossRef\]](#)
- Sapuan, S.; Leenie, A.; Harimi, M.; Beng, Y.; Sapuan, S.M. Mechanical properties of woven banana fibre reinforced epoxy composites. *Mater. Des.* **2006**, *27*, 689–693. [\[CrossRef\]](#)
- Harish, S.; Michael, D.P.; Bensely, A.; Lal, D.M.; Rajadurai, A.; Sivasankaran, H. Mechanical property evaluation of natural fiber coir composite. *Mater. Charact.* **2009**, *60*, 44–49. [\[CrossRef\]](#)
- Astarita, A.; Boccarusso, L.; Durante, M.; Viscusi, A.; Sansone, R.; Carrino, L. Study of the Production of a Metallic Coating on Natural Fiber Composite Through the Cold Spray Technique. *J. Mater. Eng. Perform.* **2018**, *27*, 739–750. [\[CrossRef\]](#)
- Jee, A.-Y.; Lee, M. Comparative analysis on the nanoindentation of polymers using atomic force microscopy. *Polym. Test.* **2010**, *29*, 95–99. [\[CrossRef\]](#)
- Liao, Q.; Huang, J.; Zhu, T.; Xiong, C.; Fang, J. A hybrid model to determine mechanical properties of soft polymers by nanoindentation. *Mech. Mater.* **2010**, *42*, 1043–1047. [\[CrossRef\]](#)
- Ferencz, R.; Sánchez, J.; Blumich, B.; Herrmann, W. AFM nanoindentation to determine Young's modulus for different EPDM elastomers. *Polym. Test.* **2012**, *31*, 425–432. [\[CrossRef\]](#)
- Shen, L.; Tjiu, W.C.; Liu, T. Nanoindentation and morphological studies on injection-molded nylon-6 nanocomposites. *Polymer* **2005**, *46*, 11969–11977. [\[CrossRef\]](#)
- Shen, L.; Wang, L.; Liu, T.; He, C. Nanoindentation and Morphological Studies of Epoxy Nanocomposites. *Macromol. Mater. Eng.* **2006**, *291*, 1358–1366. [\[CrossRef\]](#)

23. Dhakal, H.N.; Zhang, Z.Y.; Richardson, M.O.W. Nanoindentation Behavior of Layered Silicate Reinforced Unsaturated Polyester Nanocomposites. *Polym. Test.* **2006**, *25*, 846–852. [\[CrossRef\]](#)
24. Lam, C.K.; Lau, K.T. Localized elastic modulus distribution of nanoclay/epoxy composites by using nanoindentation. *Compos. Struct.* **2006**, *75*, 553–558. [\[CrossRef\]](#)
25. Aldousiri, B.; Dhakal, H.N.; Onuh, S.; Zhang, Z.; Bennett, N. Nanoindentation behaviour of layered silicate filled spent polyamide-12 nanocomposites. *Polym. Test.* **2011**, *30*, 688–692. [\[CrossRef\]](#)
26. Sánchez-Romate, X.F.; Rams, J.; Campo, M.; Jiménez-Suárez, A.; Ureña, A. Characterization of carbon nanofiber/epoxy nanocomposites by the nanoindentation technique. *Compos. Part B Eng.* **2011**, *42*, 638–644. [\[CrossRef\]](#)
27. Shokrieh, M.M.; Hosseinkhani, M.; Naimi-Jamal, M.R.; Tourani, H. Nanoindentation and nanoscratch investigations on graphene-based nanocomposites. *Polym. Test.* **2013**, *32*, 45–51. [\[CrossRef\]](#)
28. Zhu, R.; Yadama, V.; Liu, H.; Lin, R.J.T.; Harper, D.P. Fabrication and Characterization of Nylon 6/Cellulose Nanofibrils Melt-Spun Nanocomposite Filaments. *Compos. Part A Appl. Sci. Manuf.* **2017**, *97*, 111–119. [\[CrossRef\]](#)
29. Perrier, A.; Le Bourhis, E.; Touchard, F.; Chocinski-Arnault, L. Effect of water ageing on nanoindentation response of single hemp yarn/epoxy composites. *Compos. Part A Appl. Sci. Manuf.* **2016**, *84*, 216–223. [\[CrossRef\]](#)
30. Wei, G.; Bhushan, B.; Torgerson, P.M. Nanomechanical characterization of human hair using nanoindentation and SEM. *Ultramicroscopy* **2005**, *105*, 248–266. [\[CrossRef\]](#)
31. Tanguy, M.; Bourmaud, A.; Baley, C. Plant cell walls to reinforce composite materials: Relationship between nanoindentation and tensile modulus. *Mater. Lett.* **2016**, *167*, 161–164. [\[CrossRef\]](#)
32. Sair, S.; Oushabi, A.; Kammouni, A.; Tanane, O.; Abboud, Y.; El Bouari, A. Mechanical and thermal conductivity properties of hemp fiber reinforced polyurethane composites. *Case Stud. Constr. Mater.* **2018**, *8*, 203–212. [\[CrossRef\]](#)
33. Idicula, M.; Boudenne, A.; Umadevi, L.; Ibos, L.; Candau, Y.; Thomas, S. Thermophysical properties of natural fibre reinforced polyester composites. *Compos. Sci. Technol.* **2006**, *66*, 2719–2725. [\[CrossRef\]](#)
34. Zhao, X.; Wang, D.-Y.; Martin, F.H.; Zhang, X.-Q.; Wang, R.; Wang, D.-Y. Influence of phenylphosphonate based flame retardant on epoxy/glass fiber reinforced composites (GRE): Flammability, mechanical and thermal stability properties. *Compos. Part B Eng.* **2017**, *110*, 511–519. [\[CrossRef\]](#)
35. Guettler, B.E.; Moresoli, C.; Simon, L.C. Contact angle and surface energy analysis of soy materials subjected to potassium permanganate and autoclave treatment. *Ind. Crop. Prod.* **2013**, *50*, 219–226. [\[CrossRef\]](#)
36. Urai, T.; Kamai, M.; Fujii, H. Estimation of Intrinsic Contact Angle of Various Liquids on PTFE by Utilizing Ultrasonic Vibration. *J. Mater. Eng. Perform.* **2016**, *25*, 3384–3389. [\[CrossRef\]](#)
37. Chen, H.; Cheng, H.; Jiang, Z.; Qin, D.; Yu, Y.; Tian, G.; Lu, F.; Fei, B.; Wang, G. Contact Angles of Single Bamboo Fibers Measured in Different Environments and Compared with Other Plant Fibers and Bamboo Strips. *Bioresources* **2013**, *8*, 2827–2838. [\[CrossRef\]](#)
38. Oliver, W.; Pharr, G. An improved technique for determining hardness and elastic modulus using load and displacement sensing indentation experiments. *J. Mater. Res.* **1992**, *7*, 1564–1583. [\[CrossRef\]](#)
39. Hardiman, M.; Vaughan, T.J.; McCarthy, C.T. A Review of Key Developments and Pertinent Issues in Nanoindentation Testing of Fiber Reinforced Plastic Microstructures. *Compos. Struct.* **2017**, *180*, 782–798. [\[CrossRef\]](#)
40. Molazemhosseini, A.; Tourani, H.; Naimi-Jamal, M.R.; Khavandi, A. Nanoindentation and nanoscratching responses of PEEK based hybrid composites reinforced with short carbon fibers and nano-silica. *Polym. Test.* **2013**, *32*, 525–534. [\[CrossRef\]](#)
41. Zafeiropoulos, N.; Baillie, C. A study of the effect of surface treatments on the tensile strength of flax fibres: Part II. Application of Weibull statistics. *Compos. Part A Appl. Sci. Manuf.* **2007**, *38*, 629–638. [\[CrossRef\]](#)
42. Young, T., III. An essay on the cohesion of fluids. *Philos. Trans. R. Soc. Lond.* **1805**, *95*, 65–87.
43. Bargir, S.; Dunn, S.; Jefferson, B.; Macadam, J.; Parsons, S. The use of contact angle measurements to estimate the adhesion propensity of calcium carbonate to solid substrates in water. *Appl. Surf. Sci.* **2009**, *255*, 4873–4879. [\[CrossRef\]](#)
44. Fowkes, F.M. Determination of interfacial tensions, contact angles, and dispersion forces in surfaces by assuming additivity of intermolecular interactions in surfaces. *J. Phys. Chem.* **1962**, *66*, 382. [\[CrossRef\]](#)

45. Singh, S.S.; Jansen, M.A.; Franz, N.M.; Chawla, N. Microstructure and Nanoindentation of the Rostrum of *Curculio Longinasus* Chittenden, 1927 (Coleoptera: Curculionidae). *Mater. Charact.* **2016**, *118*, 206–211. [[CrossRef](#)]
46. Deng, X.; Cleveland, C.; Karcher, T.; Koopman, M.; Chawla, N.; Chawla, K. Nanoindentation Behavior of Nanolayered Metal-Ceramic Composites. *J. Mater. Eng. Perform.* **2005**, *14*, 417–423. [[CrossRef](#)]
47. Jang, J.-I.; Lance, M.; Wen, S.; Tsui, T.Y.; Pharr, G. Indentation-induced phase transformations in silicon: Influences of load, rate and indenter angle on the transformation behavior. *Acta Mater.* **2005**, *53*, 1759–1770. [[CrossRef](#)]
48. Lucca, D.A.; Herrmann, K.; Klopstein, M.J. Nanoindentation: Measuring methods and applications. *CIRP Ann.* **2010**, *59*, 803–819. [[CrossRef](#)]
49. Cocca, M.; Avolio, R.; Gentile, G.; di Pace, E.; Errico, M.E.; Avella, M. Amorphized Cellulose as Filler in Biocomposites Based on Poly(ϵ -Caprolactone). *Carbohydr. Polym.* **2015**, *118*, 170–182. [[CrossRef](#)]
50. Oushabi, A.; Sair, S.; Abboud, Y.; Tanane, O.; El Bouari, A. An experimental investigation on morphological, mechanical and thermal properties of date palm particles reinforced polyurethane composites as new ecological insulating materials in building. *Case Stud. Constr. Mater.* **2017**, *7*, 128–137. [[CrossRef](#)]



© 2020 by the authors. Licensee MDPI, Basel, Switzerland. This article is an open access article distributed under the terms and conditions of the Creative Commons Attribution (CC BY) license (<http://creativecommons.org/licenses/by/4.0/>).